Chemico-Biological Interactions 382 (2023) 110606

Contents lists available at ScienceDirect

Chemico-Biological Interactions

journal homepage: www.elsevier.com/locate/chembioint

Research paper

Rational design of novel microtubule targeting anticancer drugs N-imidazopyridine noscapinoids: Chemical synthesis and experimental evaluation based on *in vitro* using breast cancer cells and *in vivo* using xenograft mice model

Pratyush Pragyandipta [a], Ravi Kumar Pedapati [b], Praveen Kumar Reddy [b], Arnab Nayek [c], Rajesh Kumar Meher [a], Santosh Kumar Guru [d], Srinivas Kantevari [b], Pradeep K. Naik [a,*]

[a] *Centre of Excellence in Natural Products and Therapeutics, Department of Biotechnology and Bioinformatics, Sambalpur University, Jyoti Vihar, Burla, Sambalpur, 768019, Odisha, India*

[b] *Fluoro-Agrochemicals Division, CSIR-Indian Institute of Chemical Technology, Hyderabad, 500 007, India*

[c] *Department of Biochemistry, All India Institute of Medical Sciences, New Delhi, India*

[d] *Department of Biological Sciences (Pharmacology & Toxicology), National Institute of Pharmaceutical Education and Research, Hyderabad, Telangana, 500 037, India*

A R T I C L E I N F O

Keywords:
Noscapine
Molecular dynamic simulation (MD simulation)
Breast cancer
Tubulin
Anticancer agents
N-Imidazopyridine-noscapinoids

A B S T R A C T

We present N-imidazopyridine-noscapinoids, a new class of noscapine derivatives that bind to tubulin and exhibit antiproliferative activity against triple positive (MCF-7) and triple negative (MDA-MB-231) breast cancer cells. The N-atom of the isoquinoline ring of noscapine scaffold was altered *in silico* by coupling the imidazo [(Ye et al., 1998; Ke et al., 2000) 1,21,2-a] pyridine pharmacophore to rationally develop a series of N-imidazopyridine-noscapinoids (**7**–**11**) with high tubulin binding affinity. The predicted $\Delta G_{binding}$ of the N-imidazopyridine-noscapinoids **7**–**11** varied from −27.45 to −36.15 kcal/mol, a much lower value than noscapine with $\Delta G_{binding}$ −22.49 kcal/mol. The cytotoxicity of N-imidazopyridine-noscapinoids was evaluated using hormone dependent MCF-7, triple negative MDA-MB-231 breast cancer cell lines and primary breast cancer cells. The cytotoxicity of these compounds (represented as IC_{50} concentration) ranges between 4.04 and 33.93 μM against breast cancer cells without affecting normal cells (IC_{50} value > 952 μM). All the compounds (**7**–**11**) perturbed the cell cycle progression at G2/M phase and triggered apoptosis. Among all the N-imidazopyridine-noscapinoids, N-5-Bromoimidazopyridine-noscapine (**9**) showed promising antiproliferative activity and was selected for detailed investigation. The onset of apoptosis treated with **9** using MDA-MB-231 revealed morphological changes like cellular shrinkage, chromatin condensation, membrane blebbing, and apoptotic bodies formation. Along with elevated reactive oxygen species (ROS), there was a loss of mitochondrial membrane potential, suggesting induction of apoptosis to cancer cells. Compound **9** was also found to significantly regress the implanted tumour in nude mice as xenografts of MCF-7 cells without any apparent side effects after drug administration. We conclude that N-imidazopyridine-noscapinoids possess excellent potential as a promising drug for treating breast cancers.

1. Introduction

Opium alkaloid noscapine is a tubulin-bound small molecule that inhibits proliferation of cancer cells and triggers apoptosis [1]. However, it neither over-polymerizes tubulin (unlike taxanes) nor depolymerizes tubulin (vincas). In contrast, it delicately attenuates microtubule dynamics leading to activation of the mitotic checkpoints followed by the cell cycle arrest while allowing the process like axonal transport to be dependent on less microtubule dynamics [1–3]. This nature of noscapine makes it free from any significant side effects. In contrast, taxanes and vincas, cause severe side effects such as leukocytopenia, alopecia, peripheral neuropathies and diarrhoea owing to their

Abbreviations: MD, Molecular dynamics; ROS, Reactive oxygen species; RMSD, Root mean square deviation; Rg, Radius of gyration; RMSF, Root mean square fluctuation; MM-PBSA, Molecular mechanics Poisson Boltzmann surface area.

* Corresponding author.
E-mail addresses: pknaik1973@gmail.com, pknaik1973@suniv.ac.in (P.K. Naik).

https://doi.org/10.1016/j.cbi.2023.110606
Received 12 March 2023; Received in revised form 4 June 2023; Accepted 14 June 2023
Available online 15 June 2023

significant impact on microtubule organization [4–7]. Previously, it was demonstrated that noscapine and its derivatives (known as noscapinoids) have inhibited the proliferation of cancer cells of different tissue origins and reduced grafted tumours in animal models with no toxicity [1,8,9]. Moreover, it was also found to be effective against several resistant cell lines like paclitaxel (1A9/PTX10, 1A9/PTX22) and epothilone (1A9/A8) [10]. Also, its pharmacokinetics is quite favorable (get clears within 6–10 h) [11]. Due to the considerable benefits of noscapine over presently used microtubule targeting drugs, it has gained a place for usage as a potential therapeutic molecule. To increase the potentency of noscapine, we have previously developed a series of derivatives followed by chemical synthesis [12–16]. These derivatives were at various biochemical and biological assessment levels.

This study focused on developing a new series of noscapine derivatives known as N-imidazopyridine-noscapinoids (impy-noscapinoids) by strategically coupling imidazopyridine pharmacophore in the noscapine scaffold structure. After the chemical synthesis of these derivatives, their cytotoxicity was validated through cellular studies comprising two breast cancer cell lines (MCF-7 and MDA-MB-231) and primary breast cancer cells. In addition, they revealed better binding affinity with tubulin heterodimer, inhibited cell proliferation and triggered apoptosis by curtailing cellular proliferation at the G2/M phase.

2. Materials and methods

2.1. Tubulin heterodimer protein optimization

The tubulin protein (PDB ID: 6Y6D, resolution 2.20 Å) was retrieved from the protein data bank [12]. The missing hydrogen atoms in the protein structure were added by the multistep protein preparation wizard (Schrödinger, Inc., NY). With the help of the Prime (Schrödinger, Inc., NY) prediction tool, the missing side chain atoms were identified and repaired. Finally, the protein was optimized by minimizing its energy using Macromodel (Schrödinger, Inc., NY).

2.2. Rational design of novel N-imidazopyridine-noscapinoids

Imidazopyridine (the imidazole moiety linked with the pyridine ring) is a nitrogen-containing heterocycle. It is pharmacologically very active [13–15], and has antiprotozoal, antiviral, anticancer, antibacterial, analgesic, antifungal, antiinflammatory, antiapoptotic, hypnoselective, antipyretic, and anxioselective potential [16–20]. Several drugs that are in the clinics, like zolpidem **(1)** (for the treatment of insomnia), alpidem **(2)** (used as an anxiolytic drug), zolimidine **(3)** (for the treatment of peptic ulcer), necopidem **(4)** and saripidem **(5)** (used as anxiolytic drugs) and GSK812397 **(6)** (for the treatment of HIV infection) consist of imidazo [1,2-*a*] pyridine (Fig. 1) as a pharmacophore [21–24]. Therefore, in a quest to develop new series of noscapine derivatives, we have coupled the imidazo [1,2-*a*] pyridine pharmacophore with noscapine scaffold by *in silico* (Fig. 2) to design a panel of N-imidazopyridine-noscapinoids (Fig. 3). Briefly, the designed scaffold broadly has two segments (Fig. 2). The first segment is imidazo [1,2-a] pyridine, which is an active pharmacophore in most of the anticancer drugs and the second segment is the bioactive natural-α-noscapine tethered to imidazo [1,2-a]pyridine core for the desired pharmacological behavior. The imidazopyridine noscapine derivatives with varied substitutions (R-group) coupled to α-noscapine were designed based on structure activity relationship (SAR), which is a method for determining relationships between a compound's chemical structure (or structural-related properties) and biological activity (or target property). The objective of SAR is two-fold: first, to determine as accurately as possible the limits of variation in a chemical's structure concerning biological activity, and second, to define how alterations in the structure of a compound influence endpoint potency. Considering this structure-activity relationship, we first restricted the structural modifications to imidazo [1,2-a]pyridine core. Then, we made minute alterations in the structure of our targeted drug with R-groups to test their biological potency.

2.3. Preparation of molecular structure of N-imidazopyridine-noscapinoids

ChemDraw was used to draw the molecular structures of N-imidazopyridine-noscapinoids. The prepared structures were loaded in Maestro (Schrödinger, Inc., NY) and energy minimization was done by Macromodel (Schrödinger, Inc., NY) with OPLS 2005 [25], as a force

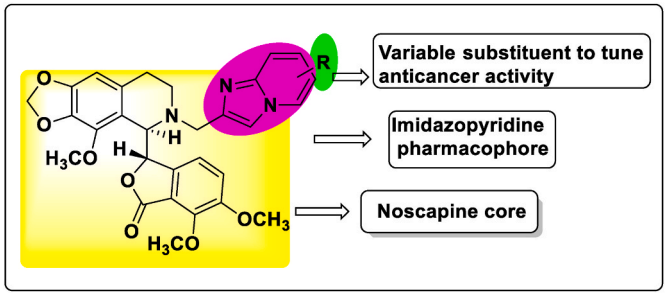

Fig. 2. General scheme for strategic development of a panel of N-imidazopyridine-noscapinoids (Impy-noscapinoids) by substitution of various functional groups at 'R'.

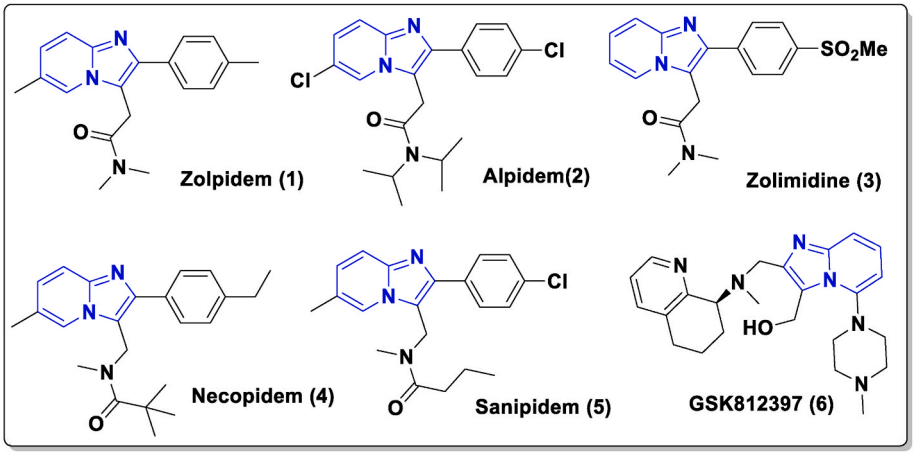

Fig. 1. Drugs in the clinics with imidazopyridine pharmacophore.

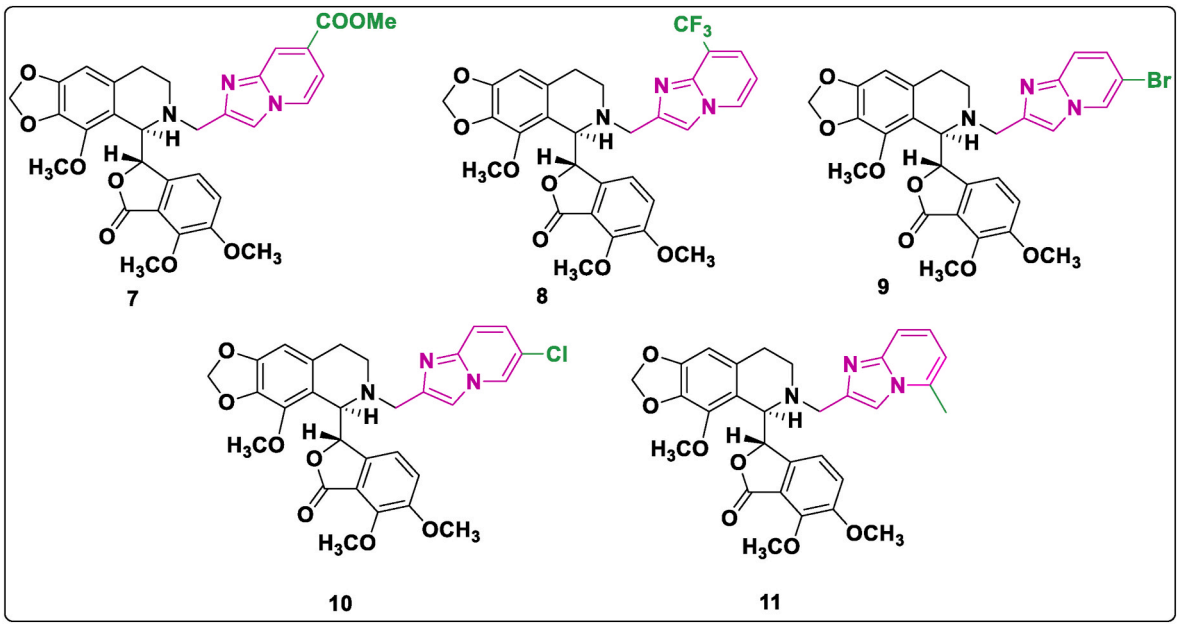

Fig. 3. The molecular structure of five Impy-noscapinoids are designed by substituting different functional groups in the imidazo [1,2-a]pyridine pharmacophore to tune anticancer activity.

field and PRCG algorithm (energy gradient of 0.001) [25]. As reported earlier, geometrical optimization was done through Jaguar (Schrödinger, Inc., NY) [26]. Various conformations of the structures were generated by Ligprep (Schrödinger, Inc., NY).

2.4. Molecular docking of N-imidazopyridine-noscapinoids

The glide algorithm (Schrödinger, Inc., NY) was used to dock the ligands (N-imidazopyridine-noscapinoids) with αβ-tubulin heterodimer, as reported earlier [27]. An inner grid box (12 Å × 12 Å x 12 Å) was generated at the midpoint of co-crystallized amino-noscapine by Glide grid-receptor generation algorithm (Schrödinger, Inc., NY). Additionally, an outer grid box (20 Å × 20 Å x 20 Å) was created where each ligand atom of a valid pose must be located. Then docking was done using Glide XP (extra precision) and all the docked poses were analyzed based on Glide XP_{Score} [28,29]. For further analysis, the optimal conformation for each ligand was considered.

2.5. MD simulation of N-imidazopyridine-noscapinoids docked complexes

Molecular dynamics (MD) simulation was carried out for the docked complex of tubulin and N-imidazopyridine-noscapinoids in the presence of GTP, GDP and magnesium by GROMACS 2019.2 version [30] as reported earlier [31]. To generate the coordinates and topology, the protein was processed by GROMACS using Amber99SB force field [32]. All the parameters (GTP, GDP, and N-imidazopyridine-noscapinoids) for each ligand were determined using a general Amber force field (GAFF) [33]. The AM1-BCC charge model was used to allot the needed atomic point charges [34]. Using tleap tool of Amber 18 and ACPYPE application [35], topologies and internal coordinates were built for all ligands. For the solvation of the complex, a distance of 12 Å between the truncated octahedron box walls and atoms of protein [31], and TIP3P as a water model was used. The system was balanced by counterions having physiological ionic strength (0.15 M). The steepest descent approach of 10000 steps was used for energy minimization to remove any conflicting contacts. Position restrictions of 10 kcal/$Å^2$ was applied for both protein and ligands before going for 500 ps NVT run at 300 K accompanied by NPT run keeping the Parrinello-Rahman barostat with a reference pressure of 1 bar for 500 ps. Following equilibration, a simulation of 100 ns with 2 fs time step was performed. Long-range electrostatic interactions were determined using the particle-mesh Ewald (PME) method. Both van der Waals and short-range electrostatics cut-offs were put at 10 Å. The Shake algorithm limited the bonds [36], while the modified Berendsen thermostat regulated the system temperature. During the MD simulation, at every 20 ps, snapshots of the atomic coordinates were taken. The sequential snapshots for Root Mean Square Deviation (RMSD), Radius of gyration (Rg) and Root Mean Square Fluctuation (RMSF) were analyzed by GROMACS and plotted by GRACE software. To explain the ligand's binding mechanism, the complex from the MD trajectory with the least total energy was used.

2.6. Prediction of binding free energy using MM-PBSA technique

The predicted binding free energy of N-imidazopyridine-noscapinoids **7**–**11** with tubulin was calculated using the Molecular Mechanics Poisson-Boltzmann Surface Area (MM-PBSA) approach [37]. From the trajectory of MD simulation, at an interval of 20 ps, 500 snapshots from the last 10 ns were taken and g_mmpbsa tool was used to determine the collective average of the $\Delta G_{bind,pred}$ [38], as follows:

$$p\Delta G_{bind,pred} = \Delta G_{complex} - \left[\Delta G_{Rec} + \Delta G_{lig}\right]$$

$$G = E_{gas} + G_{sol} - TS$$

$$E_{gas} = E_{int} + E_{ele} + E_{vdw}$$

$$G_{sol} = G_{PB(GB)} + G_{sol-np}$$

$$G_{sol-np} = \gamma SAS$$

Here G represents the Gibbs free energy. E_{gas} i.e. the gas phase energy, represents the sum of total E_{int}, (internal energy), E_{ele} (electrostatic interaction) and E_{vdw}, (van der Waals interaction energy). At the same time, the sum of G_{PB} (polar) and $G_{sol\text{-}np}$ (non-polar) contributions determine the solvation-free energy [25]. The E_{ele} (electrostatic contribution) and G_{PB} (polar solvation contribution) were added to determine the G_{PB} (Polar interaction contribution), while the $G_{sol\text{-}np}$ (nonpolar solvation contribution) is directly proportional to SAS (solvent accessible surface area) whereas γ is the surface tension constant that has

been set to 0.0072 kcal/mol [25]. Due to high predicted binding affinity towards tubulin and better docking score compared to noscapine, the five N-imidazopyridine-noscapinoids (**7**–**11**) were chemically synthesized for experimental validation.

2.7. ADME properties prediction

A total of 44 attributes responsible for absorption, distribution, metabolism, and excretion (ADME) were determined by QikProp tool (Schrödinger, Inc., NY) for the N-imidazopyridine-noscapinoids. The acceptability of the compounds was evaluated based on Lipinski's rule of 5 (number of violations of Lipinski's rule of five), i.e. quite pragmatic for drug development. When the molecule has more than five hydrogen bond donors, molecular weight is greater than 500, the log P value is more than 5 and the total N's and O's are more than 10, then a molecule is likely not qualify the Lipinski's rule of five [31], thereby leads to poor absorption or penetration.

2.8. Chemical synthesis of N-imidazopyridine-noscapinoids

We have attempted to synthesize the designed N-imidazopyridine-noscapinoids **7**–**11** chemically by strategically coupling various substituted 2-(chloromethyl) imidazo [1,2-*a*] pyridines with nor-noscapine as depicted in the synthetic scheme (Fig. 4). Natural noscapine was treated with m-CPBA to give noscapine-N-oxide, then treated with 2 N HCl to give noscapine-N-oxide.HCl salt. It is further reacted with $FeSO_4.7H_2O$ to afford nor-noscapine. To the mixture of nor-noscapine (1.0 mmol) in KI (2.0 mmol), acetone (10 mL), K_2CO_3 (2.0 mmol) and various substituted 2-(chloromethyl) imidazo [1,2-*a*] pyridine (RH; 1.1 mmol) were added gradually, and the mixture was mixed for 6h at RT. The mixture was washed in the brine solution when the reaction was completed. The organic layer was collected, moved through a Na_2SO_4 bed, and then extracted at a lower pressure. The residues were chromatographed using petroleum ether and ethyl acetate (3:1) eluents over the triethylamine silica bed to generate pure compounds **7**–**11** as white solids in 55–72% yields. The structural characterizations of intermediates and final products was performed by NMR (^1H and ^{13}C), IR spectroscopy and mass (HRMS) spectrometry. The spectra are collated in the supplementary material (S1–S15).

2.9. Cell culture and reagents

Culture media and chemicals were purchased from SIGMA. Two human breast cancer cell lines (MCF-7 & MDA-MB-231) were procured from the National Center for Cell Science's, Pune, India. The N-imidazopyridine-noscapinoids (**7**–**11**) were synthesized chemically. Stock solution (100 mM) for **7**–**11** was made using DMSO (dimethyl sulfoxide) and were preserved in 4 °C. DMEM (Dulbecco's modified Eagle medium) media supplemented with 10% fetal bovine serum (FBS; GIBCO) and antibiotics were used to culture cells at 37 °C, 5% CO_2 and 95% humidity. Trypsin-EDTA (0.25%) was used for subculturing. When cells were confluent at 70–80%, they were used for bioassays.

2.10. Cytotoxicity assay using breast cancer cell lines & primary breast cancer cells

The cytotoxicity assay for N-imidazopyridine-noscapinoids **7**–**11** and noscapine was evaluated against hormone-dependent MCF-7, triple negative MDA-MB-231 breast cancer cell lines and a panel of primary breast cancer cells obtained from our collaborator, Dr. Santosh Kumar Guru, Department of Biological Sciences (Pharmacology & Toxicology), National Institute of Pharmaceutical Education and Research, Hyderabad, India**.** Also, we have used a normal healthy human cell line, HEK to evaluate the cytotoxicity of the compounds to normal cells. Complete DMEM media supplemented with 1% pentrip (a penicillin and streptomycin mix), 2 mM 1-glutaminate and 10% FBS were used to grow cells in a T25 flask under physiological conditions of 5% CO_2 at 37 °C. After every 3–4 days, the media were changed and successive passages were done. Before the experimental study, cells were allowed to grow until they attained 70–80% confluency. In a 96 well plates, approximately 5000 cells were seeded and were treated against noscapine and N-imidazopyridine-noscapinoids **7**–**11** at a gradient concentration (5–100 μM for cancer cells and 25–400 μM for the normal cell) for 72h. The cell viability was determined based on sulforhodamine B (SRB) assay using the CellTiter96 AQueous One Solution Reagent (SIGMA) [25] and absorbance was taken at 564 nm. The IC_{50} value of noscapine and its derivatives **7**–**11** was calculated using an online tool, Quest Graph™ IC_{50} calculator (AAT Bioquest, Inc., Sunnyvale, CA, USA, https://www.aatbio.com/tools/ic50-calculator). The tool uses a four-parameters logistic regression model to calculate the IC_{50} value.

2.11. Flow cytometry analysis of cell cycle progression

DMEM media comprising 4.5 g/L glucose, 4.5 g/L L-glutamine, 1% pencillin/streptomycin and 10% FBS was used to grow MDA-MB-231 at 37 °C and 5% CO_2. Noscapine and its most potent derivative N-5-Bromoimidazopyridine-noscapine **9** dissolved in phosphate buffer saline (PBS; 1%) were treated against the cells for 72h. After treatment, the cells were analyzed by flow cytometry. About 2×10^6 cells post centrifugation were rinsed twice with PBS (ice-cold), followed by fixation with ethanol (70%), and kept in −20 °C for 24 h. After centrifugation (1000×*g*; 10 min), the supernatant was removed, followed by resuspension of pellets in 30 μl of phosphate/citrate buffer (0.2 M Na_2HPO_4/0.1 M citric acid, pH 7.5) for 30 min at RT. Following a 5 ml PBS wash, the cells were incubated for 45 min in the dark with 0.5 ml of propidium iodide (20 μg/ml in 0.6% Triton-X in PBS) and 0.5 ml of RNase A (20 μg/ml in PBS) [25]. Flow cytometer (BD FACS Aria-III) was used to analyze the samples and track the progression of the cell cycle.

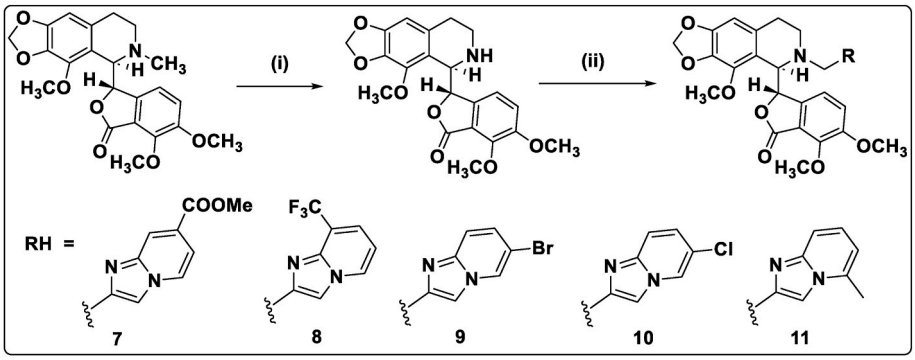

Fig. 4. Synthetic scheme 1: Scheme for chemical synthesis of imidazopyridine-noscapinoids (**7**–**11**). Reaction conditions: (i) a: m-CPBA, DCM; b: 2 N HCl; c: $FeSO_4.7H_2O$; (ii) RH, K_2CO_3, KI, acetone, rt, 4h, 60%.

2.12. Flow cytometry analysis for apoptosis assay

Apoptosis was detected using Annexin-V-FITC apoptosis detection kit (Sigma–Aldrich). In a 12 wells plate, 3×10^4 cells per well were seeded with complete media for 24h. Cells were treated with noscapine and its most potent derivative N-5-Bromoimidazopyridine-noscapine **9** for 72h against their IC_{50} concentrations. After trypsinization, cells were stained using biotin-conjugated Annexin V FITC-conjugate and propidium iodide (PI) [25]. Flow cytometer data at 488 nm excitation for PI and emission at 530 nm were collected. Viable cells (Annexin V−/PI−), early apoptotic cells (Annexin V+/PI−), late apoptotic/necrotic cells (Annexin V+/PI+) and late necrotic cells (Annexin V−/PI+) were identified and their percentage were determined.

2.13. Cellular observation by staining with fluorescent dyes

In a 6 well plates, MDA-MB-231 cells were grown over poly-L-lysine-coated coverslips and treated against IC_{50} concentration of **9** for 72 h. Coverslips were removed after incubation, fixed in cold methanol, and PBS-washed. DAPI, acridine orange (AO), Hoechst 33342 (HO), and ethidium bromide (EtBr) dyes (10 μM each) were used for staining for 15 min at room temperature and washed in PBS. The excitation and emission range were 346 nm and 460 nm, respectively. Significant morphological changes like formation of membrane blebs, nuclear condensation and apoptotic bodies were noted against the treatment of test compounds compared to untreated cells under an inverted fluorescent microscope (Nikon Eclipse Ts2R-FL).

2.14. Measurement of mitochondrial membrane potential (ΔΨm)

Rhodamine-123 (Sigma-Aldrich Co.; Ex/Em = 485 nm/535 nm), JC-1 (Invitrogen Co.; Ex/Em = 515 nm/529 nm) and DAPI (Sigma-Aldrich Co.; Ex/Em = 358 nm/461 nm) [31] dyes were used to evaluate the effect of N-5-Bromoimidazopyridine-noscapine **9** on mitochondrial membrane potential. Briefly, cells were seeded in 12 wells plates and treated against **9** for 48 h. After PBS wash, cells were stained with JC-1 (10 μg/ml) [31] for 10 min at rt. Subsequently, cells were washed with PBS twice and images were taken in an inverted fluorescence microscope (Nikon Eclipse Ts2R-FL) at 400× magnification [31]. JC-1 stained cells showed bright red fluorescence (higher ΔΨm) in untreated cells and light red fluorescence (lower ΔΨm) in treated cells. For measuring intensity image J software was used.

2.15. Intracellular reactive oxygen species (ROS) detection

Apoptosis in cancer cells can be confirmed as a result of an increase in intracellular ROS. The intracellular ROS content can be detected by the oxidative conversion of DCFH-DA (2′,7′-dichlorofluorescence-diacetate), a sensitive fluorescent probe to DCF (2′,7′-dichlorofluorescein). In a six well plates with cover glass, MDA-MB-231 cells were seeded and treated with N-5-Bromoimidazopyridine-noscapine **9** for 72 h. The cells were washed and mixed in 500 μL of DCFH-DA (10 μM; Molecular Probes Inc., Invitrogen) and incubated in the dark for 30 min at rt. Images were taken with standard excitation filters (Nikon Eclipse Ts2R-FL). The untreated control cells were observed with low green fluorescence, whereas the treated cells were observed with bright green fluorescence. The results displayed a significant rise in intracellular ROS by N-5-Bromoimidazopyridine-noscapine **9.**

2.16. In vivo antitumor efficacy against MCF-7 breast tumours

The ethical clearance for the animal study was approved by the National Institute of Pharmaceutical Education and Research (NIPER'S) Institutional Animal Ethics Committee of Hyderabad (1548/PO/Re/2011/CPCSEA). BALB/c athymic nude female mice of 8–10 weeks were kept under proper care in the Animal Care Facility. In 0.2 ml of PBS about 1×10^6 human epithelial breast adenocarcinoma, MCF-7 were dissolved and further implanted into the mice's anterior flank. Post 7–10 days, when the tumor was palpable, N-5-Bromoimidazopyridine-noscapine **9** was given by gastrogavage. The animals were randomly divided into two groups, Group 1 (control group) and Group 2 (test group), with five animals each. The Group 1 animal received regular gavage of acidified water (pH 4.0) only, while the Group 2 was treated with N-5-Bromoimidazopyridine-noscapine **9** (50 μM/day). On alternate days, tumor volume was calculated as II/6 (length x width x height) by quantifying the tumours in three transverse directions with vernier calipers [39]. Due to the large tumor volume sizes, the control group of mice were euthanized on day 30 and assigned the endpoint for control animals. The tumor size of both control and treated animals against N-5-Bromoimidazopyridine-noscapine **9** were accessed on the basis of the endpoint mentioned above.

2.17. Histopathological and hematological analyses

On the 30th day 0.2 ml of 3.5% chloral hydrate as an overdose was administrated to both the treated and the control group of mice. Blood was collected from the heart for CBC analysis (CDC Technologies, Oxford CT). In order to perfuse the animals, a mixture of 3% paraformaldehyde and 2% glutaraldehyde in PBS (pH 7.4) was used. Major organs like liver, lung, heart, kidney and tumor were removed and subjected to histological analysis after staining with hematoxylin and eosin. The tissues were examined under a microscope to assess the toxicity with the treatment of N-5-Bromoimidazopyridine-noscapine **9**.

3. Results and discussion

Numerous derivatives of noscapine were synthesized to enhance its cell-killing ability. These derivatives were found to have higher free energy of binding with tubulin, as evident from reducing their dissociation constants (K_d) substantially from 152 μM for noscapine. For example, the halogen derivatives have a K_d value of 80 to 22 μM, nitro-noscapine has 86 μM and amino-noscapine has 14 μM [27,40,41]. Furthermore, we have developed a battery of derivatives by functionalization of 'N' in the isoquinoline unit of natural α-noscapine [42] and coupling biaryl pharmacophore [43]. All these derivatives have also shown a lower K_d value compared to noscapine. This study presents a series of N-imidazopyridine-noscapinoids, **7**–**11,** as promising tubulin-binding anticancer agents.

3.1. N-imidazopyridine-noscapinoids docked well inside the binding cavity using molecular docking and MD simulation

The docking of the five N-imidazopyridine-noscapinoids **7**–**11,** and the lead molecule, noscapine, was done using Glide Xp [31]. The molecules showed well binding at the binding site. Glide XP_{score} function [28,29,31] was used to determine the binding affinity with tubulin. The N-imidazopyridine-noscapinoids, **7**–**11** revealed improved docking results varying from −8.557 to −8.082 kcal/mol than noscapine (docking score is −5.304 kcal/mol) (Table 1). Further, the docked complexes of these ligands with tubulin were taken for MD simulation (100ns) to evaluate the stability of the complexes. RMSD and Rg of the backbone C_α atoms with respect to time were analyzed by plotting the convergence of MD sequential snapshots. The relative variation for RMSD (0.21–0.24 Å) and Rg (0.966–0.972 nm) was minimal, suggesting the system's stability (Figs. 5 and 6). Further, to illustrate the suppleness of these residues, in both free form and bound form with ligands, the RMSF of the tubulin was calculated (Fig. 7a and b). The RMSF value of the residues was found to be minimum (0.02–0.04 nm) in both bound and free form for both α- and β-tubulin, revealing the rigidness of the residues. Moreover, the N-imidazopyridine-noscapinoids **7**–**11** were well accommodated within the binding site i,e at the interface of α- and β-tubulin (Fig. 8). However, as shown in ligplot the binding modes inside the binding

Table 1
Results of molecular docking of N-imidazopyridine-noscapinoids (**7**–**11**) with tubulin. All the molecules (**7**–**11**) showed better docking scores and affinity towards the tubulin than noscapine.

Ligands ID	Glide XP_{score} (Kcal/mol)	Glide Lipo (Kcal/mol)	Glide Evdw (Kcal/mol)	Glide Ecoul (Kcal/mol)	Glide Emodel (Kcal/mol)	Glide Energy (Kcal/mol)
7	−8.334	−8.697	−66.458	−7.171	−90.593	−73.630
8	−8.336	−8.869	−64.909	−6.476	−97.341	−71.386
9	−8.557	−8.583	−66.913	−7.819	−102.727	−74.733
10	−8.121	−8.578	−65.140	−5.215	−90.667	−70.355
11	−8.082	−8.393	−64.242	−6.615	−68.275	−70.858
Noscapine	−5.304	−0.589	−35.174	−7.858	−20.456	−43.032

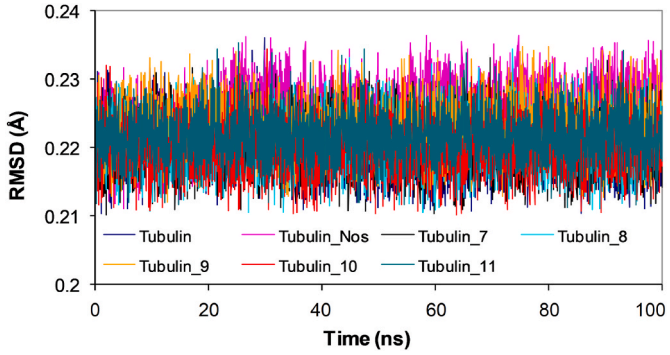

Fig. 5. RMSD of Cα carbon atoms of tubulin only and in complex with N-imidazopyridine-noscapinoids (**7**–**11**) and noscapine during 100 ns of MD simulation. During the entire period of simulation, the RMSD of the Cα atoms showed very small relative fluctuation (0.21–0.24 Å), indicating the stability of the complex.

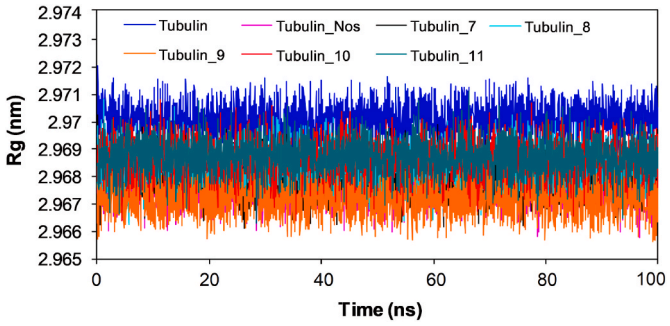

Fig. 6. Time evolution of Rg of the tubulin and in complex with N-imidazopyridine-noscapinoids (**7**–**11**) and noscapine of 100 ns of MD simulation. During the entire simulation period, the molecular systems were stable.

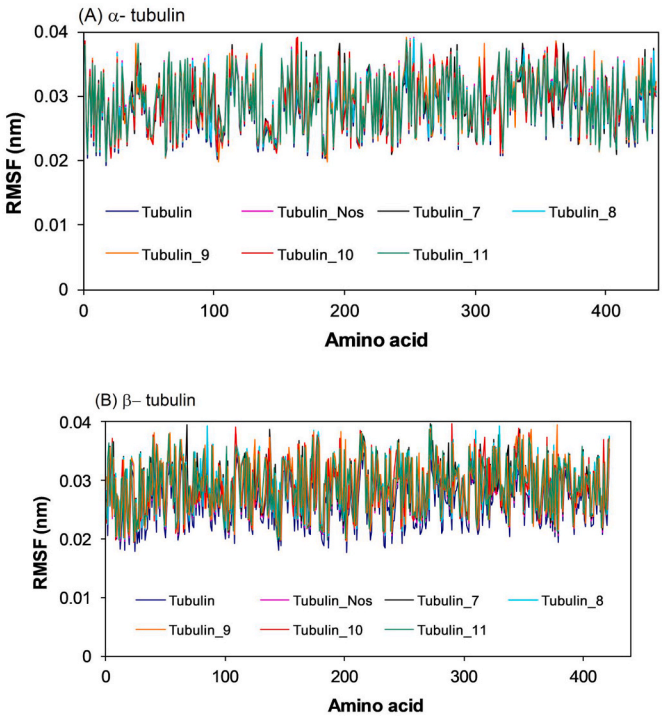

Fig. 7. a&b RMSF of the tubulin residues in both the bound and unbound states of the tubulin heterodimer with N-imidazopyridine-noscapinoids (**7**–**11**). The residues' flexibility levels varied between tubulin's free and ligand-bound forms. All amino acids showed a very low fluctuation (0.02–0.04 nm), suggesting the rigidness of residues in both free and bound form of tubulin.

cavity are unique (Fig. 9a–d). These noscapinoids have different binding modalities as different functional groups have been substituted in the scaffold structure. In the context of docking scores, the most potent N-5-Bromoimidazopyridine-noscapine **(9)** interacts more firmly with tubulin's residues than other derivatives. Its binding involved one hydrogen bond with Lys 352 (bond length 2.9 Å) (Fig. 9c). In addition to hydrogen bonding, the interaction of N-imidazopyridine-noscapinoids **(7**–**11)** with binding site residues revealed a significant number of hydrophobic interactions (Supplementary Tables S16–S19).

3.2. N-imidazopyridine-noscapinoids showed high binding free energy with tubulin

The predictive binding free energy ($\Delta G_{bind,PBSA}$) of N-imidazopyridine-noscapinoids, **7**–**11** and noscapine with tubulin is shown in Table 2 based on MM-PBSA approach. For each tubulin-noscapinoid complex, the binding free energy value was determined in accordance with the mean value out of 1000 snapshots taken during the last 2ns of the MD trajectory. It was revealed that the N-imidazopyridine-noscapinoids, **7**–**11** have a stronger binding affinity with tubulin than noscapine. Among all the derivatives, N-5-Bromoimidazopyridine-noscapine **(9)** showed the highest binding energy of −36.15 kcal/mol. The intermolecular van der Waals (ΔE_{vdw}) and the electrostatic (ΔE_{ele}) are excellent contributors to the binding, while the polar solvation terms (ΔG_{polar}) counteract binding. The solvent accessible surface area term (ΔG_{SASA}), nevertheless, contributed favorably but marginally.

3.3. Predicted ADME properties of noscapine and its N-imidazopyridine-noscapinoids, 7-11

We have predicted the ADME properties of N-imidazopyridine-noscapinoids, **7**–**11** using QikProp (Schrödinger, Inc., NY). Several attributes like molecular weight (MW), total solvent accessible surface area (SASA), octanol/water partition coefficient (QPlogPo/w), octanol/gas partition coefficient (QPlogPoct), water/gas partition coefficient (QPlogPw), polarizability in cubic angstroms (QPlogrz), % human oral absorption in intestine (QP%), brain/blood partition coefficient (QPlogBB), IC_{50} value for blockage of HERG K+ channel (QPlogHERG), skin permeability (QPlogKp), prediction of binding to human serum albumin (QPlogKhsa), apparent Caco-2 cell permeability in nm/sec

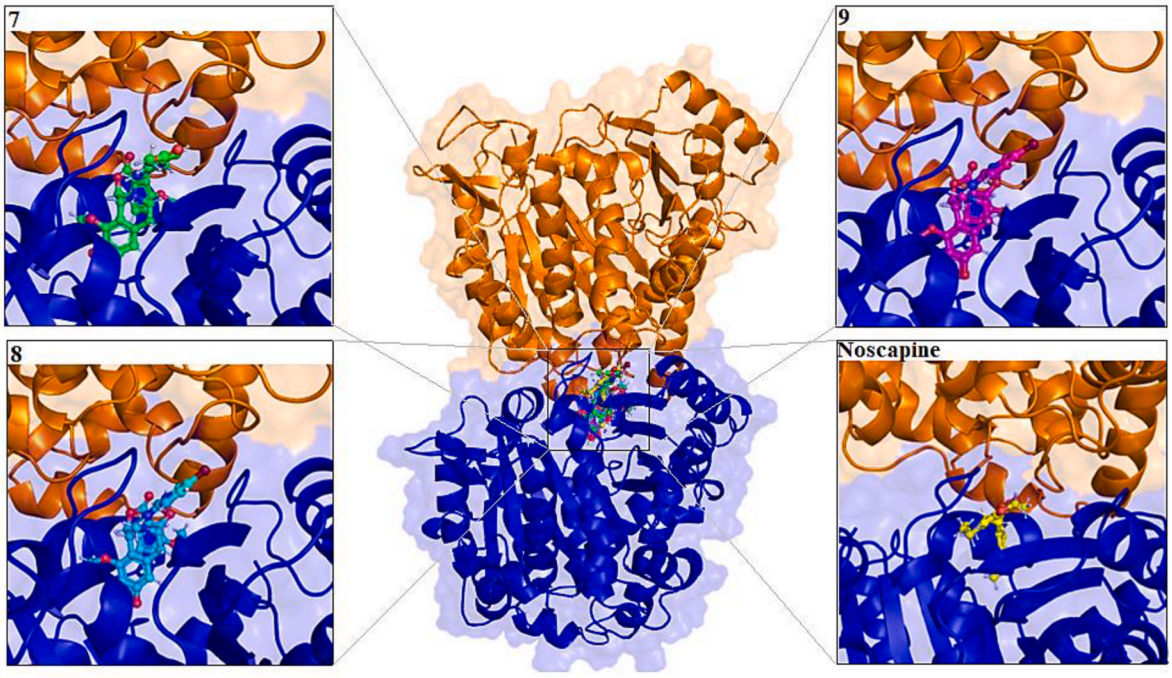

Fig. 8. N-imidazopyridine-noscapinoids (**7**–**9**) & Noscapine are well encased within the binding site i.e. at the interface of α- and β-tubulin. The macromodel surface approach based on α- and β-tubulin (brown colour denotes α-tubulin and blue colour denotes β-tubulin) show the binding site.

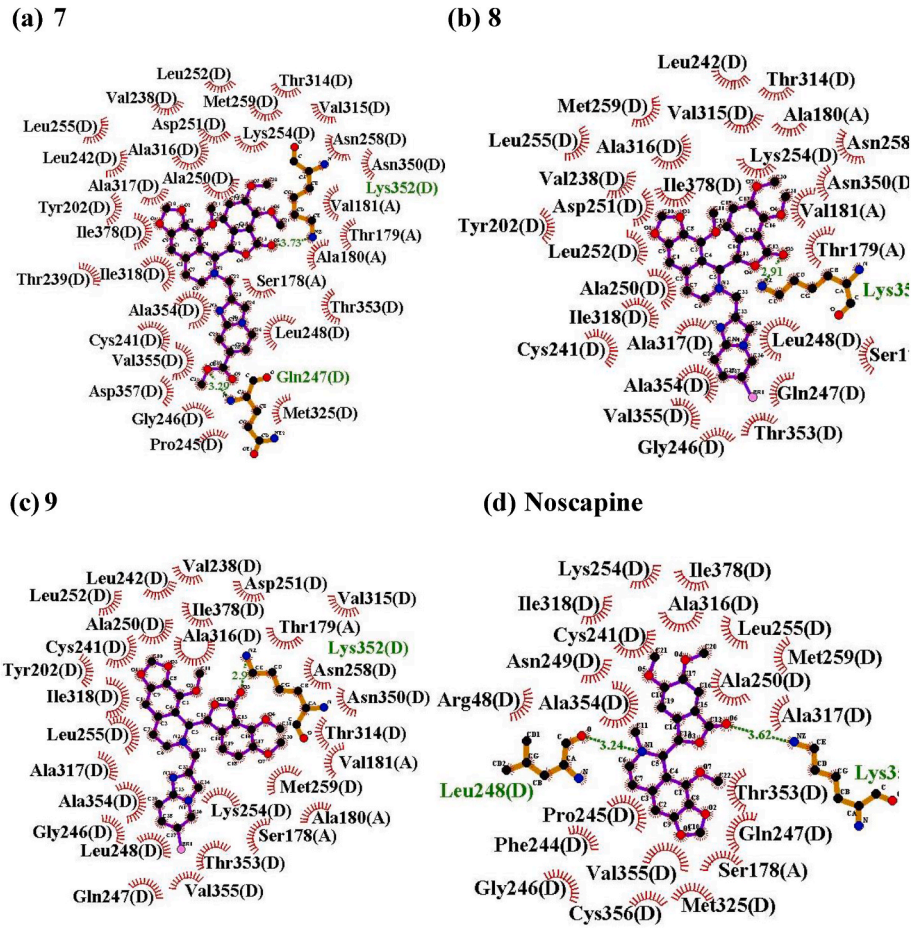

Fig. 9. Two-dimensional illustration of the interaction between the N-imidazopyridine-noscapinoids, **(a) 7, (b) 8, (c) 9 and (d) noscapine** with the binding site residues of tubulin. The dashed lines are the hydrogen bonds and bond lengths in Å. The representation of hydrophobic interactions is an arc with radial spokes. LIGPLOT software was used to make the figures. The residues that were 5 Å away from the docked ligands are only shown.

Table 2
Predictive binding free energy calculated (Kcal/mol) for the N-imidazopyridine-noscapinoids, **7**–**11** & Noscapine with αβ tubulin dimer.

N-imidazopyridine-noscapinoids_Tubulin	ΔE_{vdw} (Kcal/mol)	ΔE_{elec} (Kcal/mol)	ΔG_{polar} (Kcal/mol)	ΔG_{SASA} (Kcal/mol)	$\Delta G_{binding}$ (Kcal/mol)
7	−53.12	−21.02	48.55	−4.46	−30.05
8	−55.21	−20.29	48.20	−4.28	−31.58
9	−61.53	−23.17	54.45	−5.87	−36.12
10	−52.81	−20.42	49.28	−5.02	−28.97
11	−49.27	−20.88	47.44	−4.74	−27.45
Noscapine	−46.34	−18.23	46.48	−4.85	−22.94

(QPPCaco) and apparent MDCK cell permeability in nm/sec (QPPMDCK) [25]. Caco-2 cells serve as the gut-blood barrier model, while MDCK cells are regarded as an excellent replica of the blood-brain barrier. Lipinski's rule of 5 (number of violations of Lipinski's rule of five), vital for drug design was used to validate the acceptability of noscapine and its N-imidazopyridine-noscapinoids, **7**–**11**. Surprisingly noscapine and its N-imidazopyridine-noscapinoids, **7**–**11** showed substantial values for the properties analyzed and also passed Lipinski's rule of 5 (Table 3).

3.4. Cytotoxicity study in breast cancer cell lines

Cytoxicity evaluation for noscapine and its N-imidazopyridine-derivatives, **7**–**11** was done against hormone-dependent MCF-7 and triple negative MDA-MB-231 cell lines. All the N-imidazopyridine-derivatives, **7**–**11** exhibited potent cytotoxic activity against the above cell lines when treated with gradient concentrations compared to noscapine (Fig. 10). The IC_{50} values for **7**–**11** for both cell lines are shown in Table 4. The IC_{50} values were found to be statistically significant compared to untreated cells ($p < 0.05$). Surprisingly, noscapine and its N-imidazopyridine-derivatives **7**–**11** inhibited the proliferation of normal healthy cells with IC_{50} value > 952 μM, suggesting that these compounds are non-toxic to normal healthy cells (Table 4 and Fig. 11). Among all the derivatives, N-5-Bromoimidazopyridine-noscapine **(9)** showed promising cytotoxicity using both the cell lines (IC_{50} value is 5.26 μM against MCF-7 and 7.78 μM against MDA-MB-231) and was selected for the detailed investigation. The relative IC_{50} values obtained suggest that these noscapinoids inhibit the proliferation of cancer cells independent of hormone receptor status. Although a definitive link between the selectivity of cancer cells to these derivatives has not yet been established, it is evident that tubulin could be a good target for these derivatives.

3.5. Cytotoxicity of N-imidazopyridine-noscapinoids, 7–11 on primary breast tumor cells

Further, the cytotoxicity of N-imidazopyridine-noscapinoids, **7**–**11** and noscapine in primary breast tumor cells was evaluated. All the N-imidazopyridine-noscapinoids exhibited potent cytotoxic compared to noscapine at an increasing concentration (Fig. 12). The IC_{50} values are collated in Table 5. The IC_{50} value against the primary breast cancer cells ranges from 11.82 to 32.64 μM for noscapine, 6.86–18.46 μM for **7,** 5.55–11.68 μM for **8**, 4.04–4.93 μM for **9**, 4.27–4.89 μM for **10**, and 5.22–8.37 μM for **11** (Table 5).

3.6. N-5-Bromoimidazopyridine-noscapine (9) induced apoptosis to cancer cells

Apoptosis in triple negative breast cancer cell line was evaluated against treatment with N-5-Bromoimidazopyridine-noscapine (**9**). During apoptosis, there is a change in the lipid composition i.e., the phosphatidylserine translocated from inner leaflet to outer leaflet. The phosphatidylserine translocation to the outer membrane was detected by annexin V binding. Likewise, the cell-impermeant DNA-binding fluorescent propidium iodide dye can only enter the cells when membrane permeability is compromised i.e., in the late stages of apoptosis. Using the fluorescent dyes, early and late apoptotic cells were quantified by FACS. The percentage of early apoptotic and late apoptotic cells against the treatment of N-5-Bromoimidazopyridine-noscapine **(9)** at an IC_{50} concentration (7.8 μM) for 72h is collated in Fig. 13. Only a few early (2%) and late (3%) apoptotic cells seen in the control after 72h were considered as background cell death due to regular stress (Fig. 13a). In contrast, the early apoptotic cells (15%) and late apoptotic cells (20% and 15% necrotic cells) with treatments of N-5-Bromoimidazopyridine-noscapine **(9)** were found to be significantly more compared to controlled untreated cells (Fig. 13b).

3.7. Detection of apoptosis with treatment of N-5-Bromoimidazopyridine-noscapine (9)

Several morphological changes occur during apoptosis, but mainly membrane blebbing, chromatin condensation, cellular shrinkage, and formation of apoptotic bodies are seen. AO, HO & EtBr stains are used to evaluate the induction of apoptosis by N-5-Bromoimidazopyridine-noscapine (**9**) when treated against MDA-MB-231. The untreated cells showed no signs of morphological changes, while in the case of treated cells, there were numerous fragmented nuclei, membrane blebbing and apoptotic bodies (Fig. 14).

Table 3
ADME attributes calculated for N-imidazopyridine-noscapinoids and noscapine by Qikprop. N-imidazopyridine-noscapinoids 7–11 and noscapine satisfied all the properties vital for ADME screening.

Sl No	ADME Screening	7	8	9	10	11	Noscapine	Recommended values
1	MW.	587.58	608.44	608.44	563.99	543.57	413.42	130–725
2	SASA	856.44	748.17	772.45	787.75	801.82	597.02	300–1000
3	Accpt HB	12.25	10.25	10.25	10.25	10.25	8.75	2.0–20.0
4	QPpolrz	57.49	51.86	52.78	53.41	53.97	39.09	13.0–70.0
5	QPlogPoct	26.58	23.55	23.75	23.88	23.57	17.81	8.0–35
6	QPlogPw	15.06	12.54	12.65	12.86	12.72	10.08	4.0–45.0
7	QPlogPo/w	2.82	3.54	3.64	3.70	3.54	1.79	−2.0-6.5
8	QPlogHERG	−6.96	−6.01	−6.31	−6.61	−6.64	−4.42	Below −5.0
9	QPPCaco	150.7	670.2	585.0	541.8	571.4	777.7	<25 poor >500 great
10	QPlogBB	−0.79	0.27	0.18	0.12	−0.039	0.33	−3.0-1.2
11	QPPMDCK	70.80	917.73	790.29	699.29	298.91	417.06	<25 poor >500 great
12	QPlogKp	−4.50	−3.37	−3.48	−3.46	−3.49	−3.95	−8.0–−1.0
13	QPlogKhsa	−0.18	−0.05	0.008	0.038	0.093	−0.49	−1.5-1.5
14	Rule of Five (No. of violations)	2	3	2	2	2	3	Maximum is 4

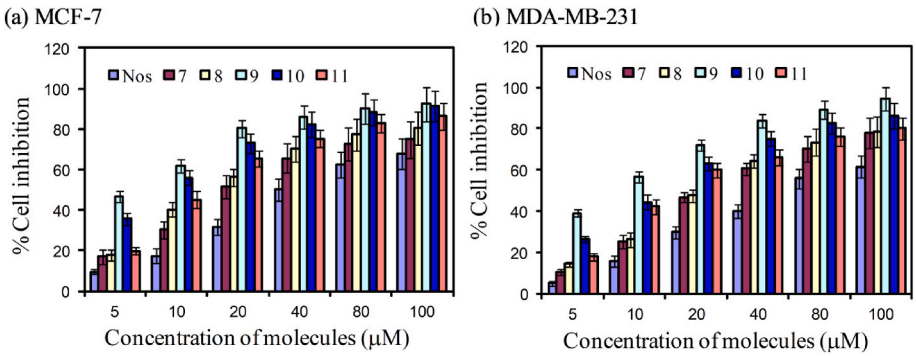

Fig. 10. The N-imidazopyridine-noscapinoids **7**–**11** have more cytotoxicity compared to noscapine using human breast cancer cells. Noscapine and its imidazopyridine-noscapinoids, **7**–**11** were treated against (A) MCF-7 and (B) MDA-MB-231 for 72 h. The experiment was done thrice and the values are the mean of those.

Table 4
IC_{50} values of N-imidazopyridine derivatives of noscapine using breast adenocarcinoma cell lines and a normal cell line (HEK). Compared to noscapine all the potent derivatives showed better cytotoxicity to cancer cells, without any significant effect on the normal healthy cell line. The statistical significance of the IC_{50} ($p < 0.05$) values between treated and untreated was determined using student t-test. The IC_{50} value was calculated using an online tool, Quest Graph™ IC_{50} calculator (https://www.aatbio.com/tools/ic50-calculator), which uses a four-parameters logistic regression model to calculate the IC_{50} value.

IC_{50} (μM)						
	Noscapine	7	8	9	10	11
MCF-7	28.7 ± 2.53*	13.22 ± 1.48*	11.22 ± 1.72*	5.26 ± 0.64*	7.37 ± 0.76*	9.89 ± 0.92*
MDAMB-231	33.93 ± 4.02*	17.24 ± 1.52*	17.15 ± 1.62*	7.78 ± 0.84*	10.3 ± 0.63*	9.95 ± 0.52*
HEK	952.0 ± 5.64*	1648.9 ± 7.84*	1768.7 ± 7.5*	1510.4 ± 5.24*	2249.7 ± 6.37*	1703.5 ± 5.29*

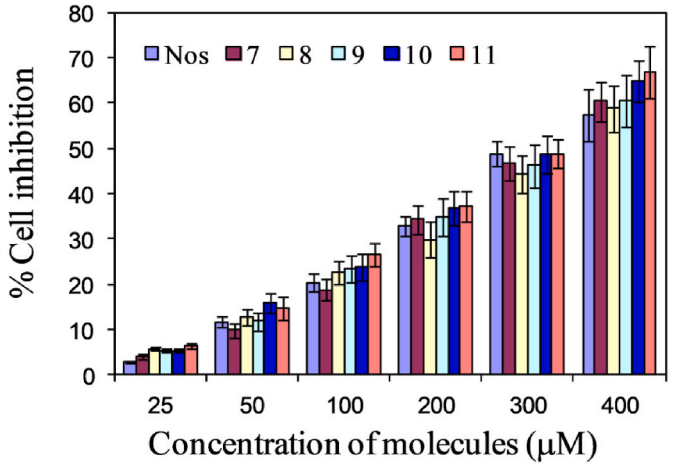

Fig. 11. Noscapine and its N-imidazopyridine-noscapinoids **7**–**11** (25–400 μM) effect on cell viability of normal healthy cell (HEK).

3.8. Effects of N-5-Bromoimidazopyridine-noscapine (9) on ROS accumulation in MDA-MB-231 cells

Additionally, we found that N-5-Bromoimidazopyridine-noscapine **(9)** elevated ROS levels by triggering apostosis in cancer cells. To evaluate the ROS levels DCFDA a molecular probe was taken into account. When cells (MDA-MB-231) were treated against **9** the green fluorescence was more intense compared to untreated cells (Fig. 15a). We found that **9** significantly elevated ROS levels in MDA-MB-231 cells as measured by fluorescent intensity, suggesting that for inducing apoptosis, the ROS might have a function (Fig. 15b).

3.9. N-5-Bromoimidazopyridine-noscapine (9) arrested the cell cycle at G2/M phase

N-5-Bromoimidazopyridine-noscapine **(9)** when treated with its IC50 concentration (7.8 μM) against triple-negative breast cancer cell line arrested the cell cycle at G2/M phase (Fig. 16). A deposition of fluorescently labeled DNA within the cell is a good marker of how cell cycle progression and cell death are impacted. G1 phase is represented by 2 N DNA, while G2 and M phases are characterized by 4 N DNA. S phase is indicated by the process when the cells undergo duplication between the 2 N and 4 N peaks. Cells falling short of 2 N DNA are apoptotic cells with degraded DNA to varying degrees. It was observed that when MDA-MB-231 cells were treated with N-5-Bromoimidazopyridine-noscapine (**9**) at its IC_{50} concentration (7.8 μM) for 72h, it induced substantial changes in the cell cycle profile. High accumulation was seen at G2/M phase when treated against N-5-Bromoimidazopyridine-noscapine (**9**) for 72h compared to the untreated cells. A distinctive hypodiploid DNA content peak (sub-G1) was found to be increased after 72h of drug treatment, contrary to G2/M block. More number of cells with hypodiploid DNA content signify more dying cells.

3.10. Effects of N-5-Bromoimidazopyridine-noscapine (9) on mitochondrial membrane potential (ΔΨm)

Mitochondria are known to be the main pathway for apoptosis. A collapse in mitrochondrial membrane potential (**Δ**Ψm) is likely to be related to triggering apoptosis. Keeping this in mind the mitochondrial membrane potential (**Δ**Ψm) loss was measured in triple negative breast cancer cell line, treated with N-5-Bromoimidazopyridine-noscapine **(9)** and stained with dyes JC-1. The treatment of **9** against MDA-MB-231 cells showed less intense red fluorescence than untreated cells (Fig. 17), indicating that compound **9** significantly increased the mitochondrial membrane potential (ΔΨm) loss in triple negative breast cancer cell line.

3.11. Reduction in tumor volume with the treatment of N-5-Bromoimidazopyridine-noscapine (9) against MCF-7 xenograft model

Treatment with N-5-Bromoimidazopyridine-noscapine **(9)** at a dose of 50 μM/day significantly reduced the tumor volume in the treated than control ($P < 0.001$) (Fig. 18A). On day 40 post tumour implantation the tumour volume was decreased by 809 mm^3 from the untreated control group with tumour volume 1479 mm^3. Mice were euthanized and tumours were removed and weighed on 40th day. Solid tumours of various weights ranging between 4.8 and 11.2 g (mean 7.9 ± 2.0 g) were seen in the case of all untreated mice. In contrast, the tumour weight

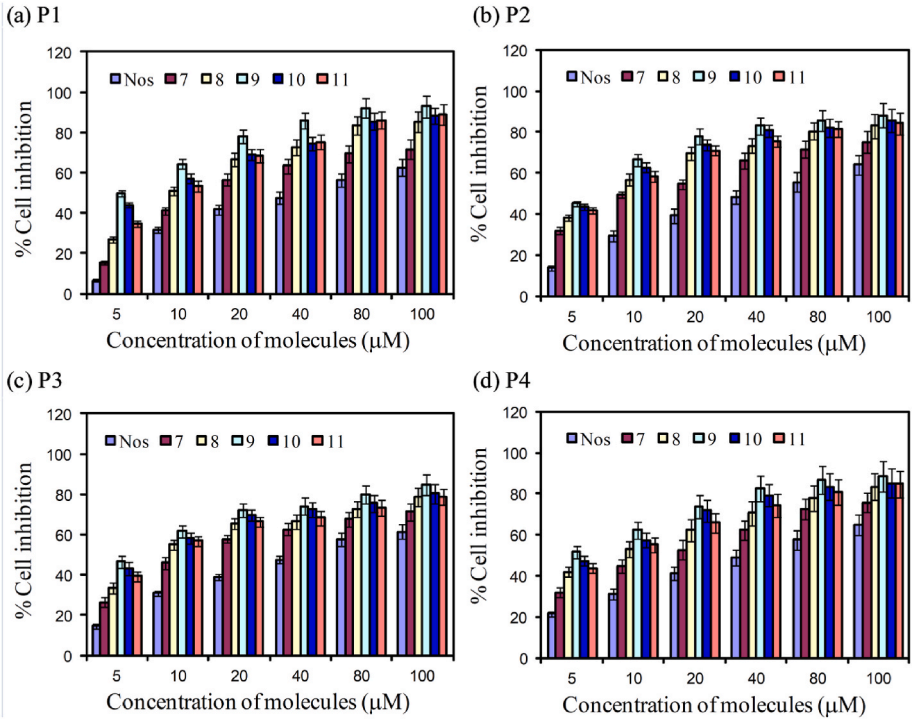

Fig. 12. The N-imidazopyridine-noscapinoids, **7**–**11** inhibits cell proliferation of human primary breast tumor cells more effectively compared to noscapine. N-imidazopyridine-noscapinoids, **7**–**11** and noscapine were treated against primary breast cancer cells for 72h. The experiment was done thrice and the values are the mean of those.

Table 5
The IC_{50} values of N-imidazopyridine-noscapinoids, **7**–**11** and noscapine when treated against primary breast cancer cells isolated from different patients' breast tumor tissue. The N-imidazopyridine-noscapinoids, **7**–**11** exhibited more cytotoxicity than noscapine. The statistical significance of the IC_{50} ($p < 0.05$) values between treated and untreated was determined using a student t-test.

IC_{50} (μM)						
Patients No.	**Noscapine**	**7**	**8**	**9**	**10**	**11**
1	11.82 ± 1.54*	9.02 ± 1.62*	8.36 ± 1.83*	4.93 ± 0.69*	7.74 ± 1.58*	8.37 ± 1.47*
2	16.67 ± 1.85*	7.75 ± 1.72*	5.66 ± 1.82*	4.74 ± 1.29*	4.80 ± 0.84*	5.22 ± 1.17*
3	16.09 ± 3.48*	6.86 ± 1.28*	5.55 ± 1.45*	4.04 ± 1.37*	4.27 ± 1.54*	4.67 ± 1.63*
4	32.64 ± 3.15*	18.46 ± 1.38*	11.68 ± 1.71*	4.35 ± 0.35*	4.89 ± 0.68*	6.95 ± 0.87*

dramatically decreased in the treated groups, and only a few palpable tumours were observed. The tumour growth suppression by N-5-Bromoimidazopyridine-noscapine (**9**) was statistically significant ($p < 0.001$) in comparison to the untreated control mice. Additionally, after drug treatment, we did not observe any noticeable weight loss compared to the control group (Fig. 18B).

3.12. Treatment of N-5-Bromoimidazopyridine-noscapine (9) showed no toxicity

The adverse toxicity of chemotherapeutic drugs is a serious concern during cancer treatment. Clinically approved microtubule-targeting drugs like vinca alkaloids and taxanes also show severe side effects [4]. Hence, there is an urge to find a drug regimen that is stable and well-tolerated. To evaluate whether N-5-Bromoimidazopyridine-noscapine (**9**) is toxic to healthy tissues, we analyzed tumor-bearing mice's liver, kidney, heart, and lungs. Treatment with **9** fails to show any pathological aberrations in normal tissues. A 5.0 micron-thick section of the liver, kidney, lung, and heart was stained with H&E, embedded with paraffin, and visualized at 200× magnification (Fig. 19). The structure of the hepatic lobules was normal. The kidneys had normal glomeruli, interstitium, proximal and distal tubule and blood arteries. The heart muscles in each group had the usual morphology. In the lung tissue, normal alveoli and bronchial airways have been observed. In the context of hematological parameters, no variations were found between treated and control animals (Tables 6 and 7).

4. Conclusion

To conclude, we have strategically developed a series of N-imidazopyridine-noscapinoids from noscapine to increase its anticancer potency. At the same time, we have also come up with the most straightforward synthetic scheme for synthesizing N-imidazopyridine-noscapinoids in high yields from the lead molecule, noscapine, through direct and regioselective mode. Using MCF-7 and MDA-MB-231 breast cancer cell lines and primary breast cancer cells, all five derivatives exhibited potent cytotoxicity without affecting normal healthy cells. The most promising compound, N-5-Bromoimidazopyridine-noscapine **(9)**, also revealed a significant reduction in the volume of implanted tumour based on *in vivo* xenograft mice model without any toxic effects to vital organs. Therefore, these novel microtubule-targeting congeners will be effective against breast cancers and beneficial against other forms of cancer.

Ethical approval

The Institutional Animal Ethics Committee of the National Institute of Pharmaceutical Education and Research (NIPER), Hyderabad (1548/PO/Re/2011/CPCSEA) approved the study.

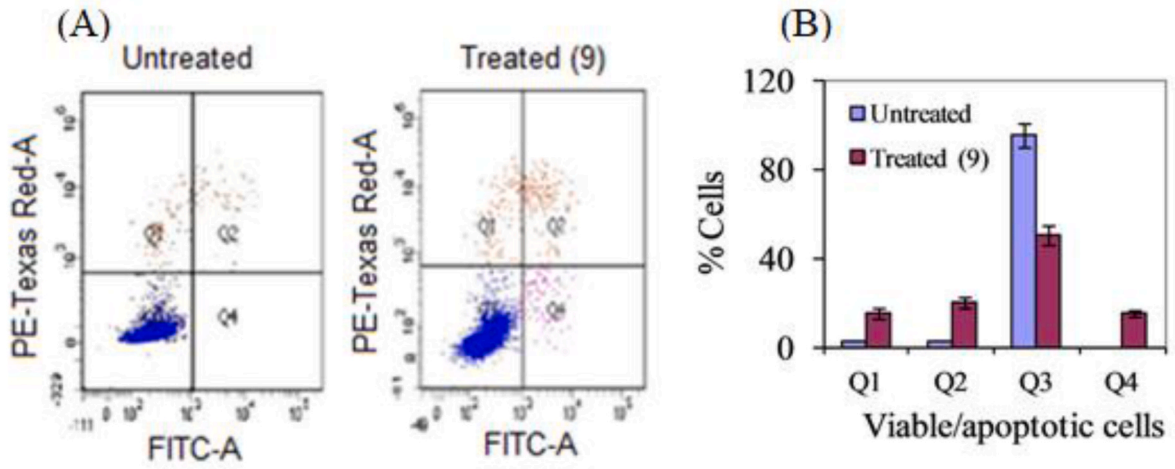

Fig. 13. Flow cytometry analysis of apoptotic cells using MDA-MB-231 cells treated with N-5-Bromoimidazopyridine-noscapine **(9)** with IC_{50} concentration (7.8 μM) for 72 h and compared with non-treated control cells. The three sub-populations: PI-negative and Alexa Fluor 488-negative viable cells with intact membrane and preserved amino-phospholipid asymmetry (PI-, Alexa Fluor 488-), PI-negative and Alexa Fluor 488-positive early apoptotic cells with intact cellular membrane exposing phosphatidylserine (PI-Alexa Fluor 488+), and PI-positive and Alexa Fluor 488-positive late apoptotic cells with compromised asymmetry and membrane permeability (PI+, Alexa Fluor 488+) were differentiated by the use of Alexa Fluor 488 conjugate of Annexin-V along with propidium iodide (PI) dye. Representative results of three independent experiments. (B) Percentage of viable (Q3), early apoptotic (Q1), late apoptotic (Q2) and necrotic (Q4) cell measured by flow cytometry.

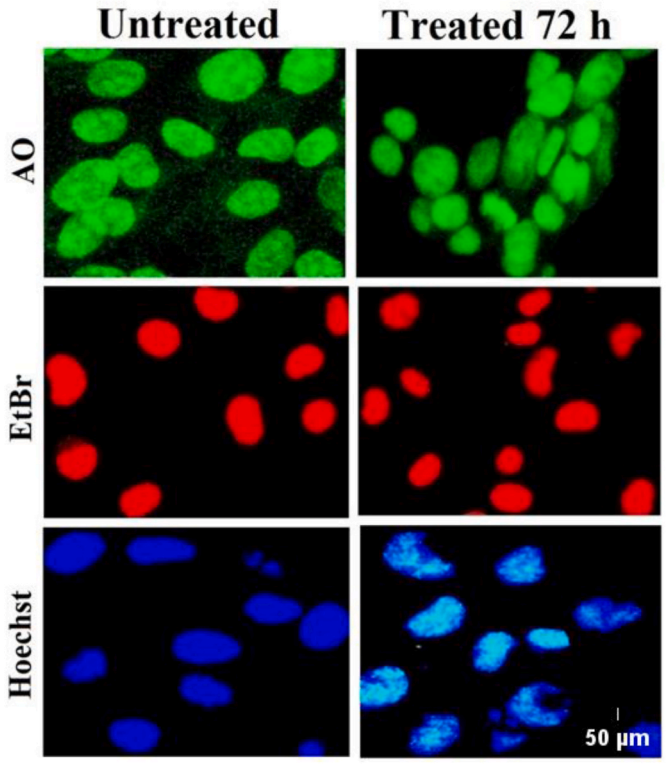

Fig. 14. Apoptotic cells were identified by morphological characteristics changes like chromatin condensation, blebbing of the plasma membrane, and forming smaller, apoptotic entities. Panel shows cells stained with AO, HO & EtBr, revealing morphological features between untreated cells and cells treated with IC50 concentration (5.3 μM) of N-5-Bromoimidazopyridine-noscapine **(9)** for 72h using fluorescence microscopy. After 72h of drug treatment, the apoptotic cancer cells were evident.

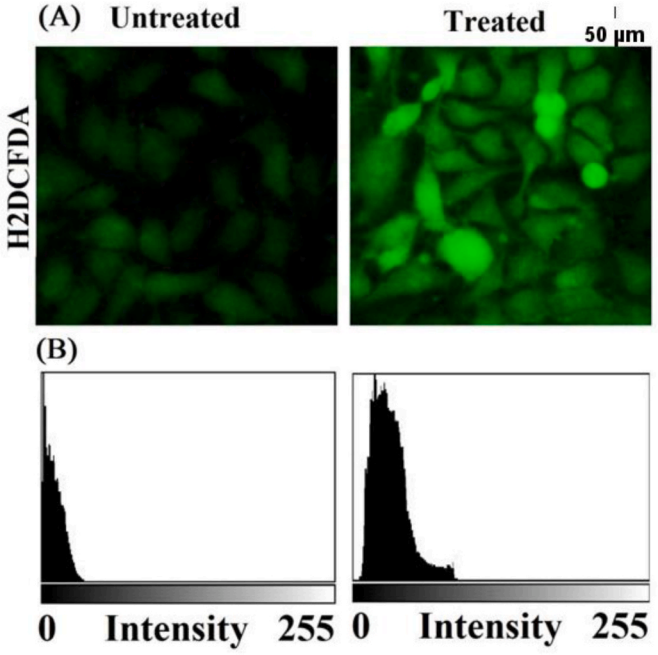

Fig. 15. (A) Treatment at IC_{50} concentration (7.8 μM) the N-5-Bromoimidazopyridine-noscapine **(9)** derivative elevated the ROS level against MDA-MB-231 cells compared to untreated cells as measured by the fluorescent dye DCFDA. (B) Image J was used to measure the intensity.

Author's contibution

PP has performed most of the computational and biological experiments and written the initial draft of the manuscript. RP and PR have chemically synthesized the designed derivatives and elucidated their structures. AN has performed the MD simulation of the docked complexes and calculated the predicted binding energy. RM has performed the cell cycle progression and apoptosis assays. SG has conducted the *in vivo* animal study using nude mice. SK has conceptualized the design of novel derivatives and synthetic schemes for the synthesis of the derivatives. PKN has conceptualized the entire study and edited the manuscript.

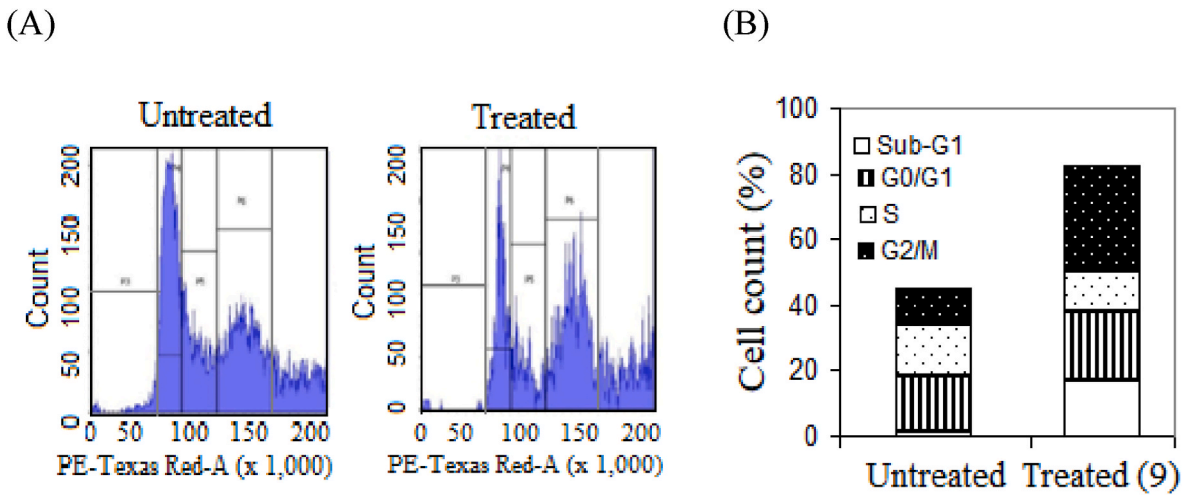

Fig. 16. Treatment with N-5-Bromoimidazopyridine-noscapine **(9)** at its IC_{50} concentration (7.8 μM) arrested the cell cycle at G2/M and revealed a hypodiploid (sub-G1) DNA peak indicating apoptotic cells. A) Flow Cytometry analysis of cell cycle progression against the treatment of N-5-Bromoimidazopyridine-noscapine (**9**) at a 25 μM in MDA-MB-231 cells after 72 h B) Different phases of cell cycle showing the percentage of cells at each stage.

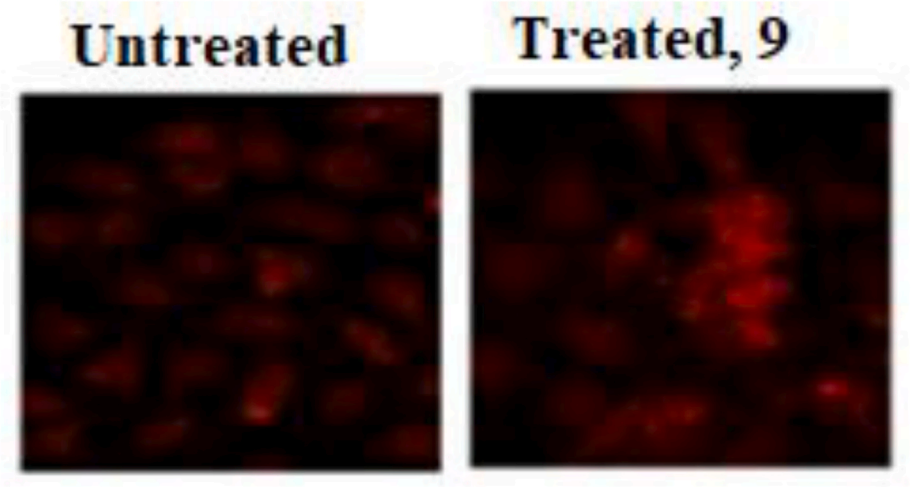

Fig. 17. Effect on mitochondrial membrane potential by N-5-Bromoimidazopyridine-noscapine **(9)** stained with JC-1 fluorescent dye. Compound **9** significantly increased the loss of mitochondrial potential of MDA-MB-231 cells.

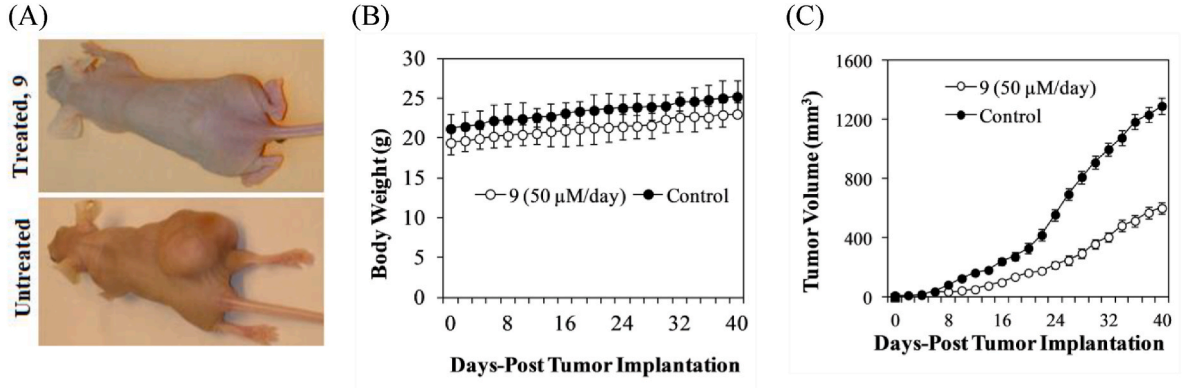

Fig. 18. Orally administered N-5-Bromoimidazopyridine-noscapine **(9)** efficiently reduces the tumour volume compared to untreated groups. Preestablished palpable tumour-bearing mice were randomly chosen and divided into two groups as described in materials and methods. (A) representative example of untreated control and compound **9**-treated animal with such xenografted tumours. (B) Effect on the body weight of mice. No difference in body weight was noticed between the treated and untreated mice. (C) Progression in tumour growth on human MCF-7 xenograft mice with the treatment of **9**. The tumour growth was significantly inhibited by N-5-Bromoimidazopyridine-noscapine **(9)** compared to untreated group.

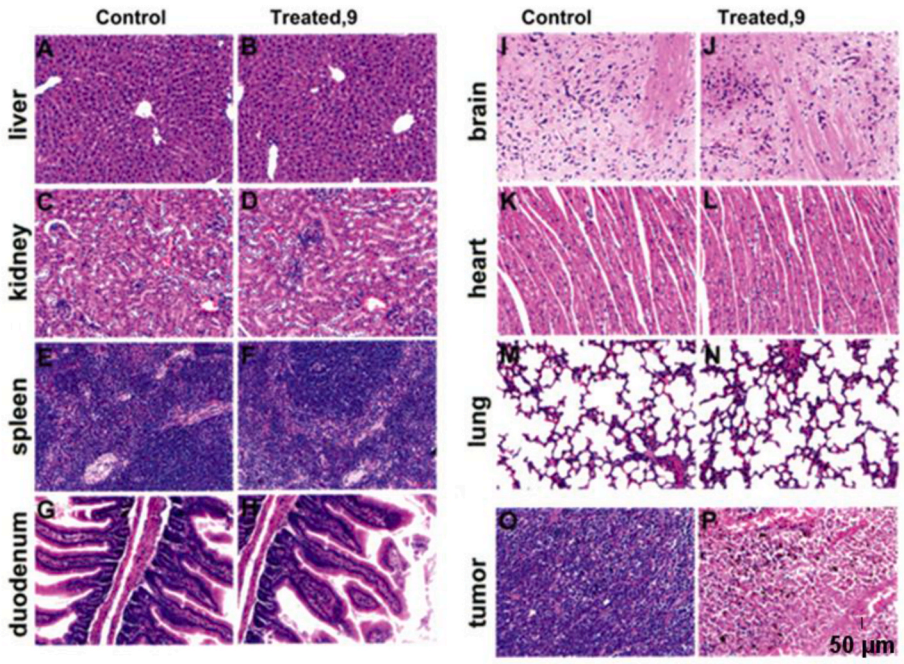

Fig. 19. Panels represent H&E staining of paraffin-embedded 5 micron-thick sections of the liver, kidney, spleen, duodenum, brain, heart and lung at 200× magnifications. The normal hepatic lobular structure was found in the liver. The proximal and distal tubules, interstitium, normal glomeruli and blood arteries in the kidneys were normal. The splenic follicles and vascular sinusoids of the **9**-treated and vehicle-treated control groups were identical. The heart muscle had normal shape between the two groups, and the lung tissue revealed normal alveoli. The cerebral cortex and the white and gray matter appeared to be healthy. The mucosa, submucosa, and muscularis mucosa in the gut were all normal.

Table 6
Hematological parameters, WBC count (WBC), monocytes (MON), eosinophils (EOS), RBC count (RBC), haemoglobin concentration (HB), Hematocrit (HCT), mean corpuscular volume (MCV), mean corpuscular hemoglobin (MCH), mean corpuscular hemoglobin concentration (MCHC) and platelet count between the treated (50 μM/day) and control groups.

Parameter	Treated (50 μM/day)	Control
WBC (10^3/μl)	3.6 ± 2.8	3.2 ± 2.1
MON (%)	0.6 ± 0.01	0.5 ± 0.08
EOS (%)	0.8 ± 0.09	0.7 ± 0.08
RBC (10^6/μl)	4.49 ± 0.5	4.6 ± 0.7
HB (g/dl)	18.3 ± 0.6	17.8 ± 0.4
HCT (%)	42.5 ± 1.2	43.1 ± 0.8
MCV (fL)	64.7 ± 0.7	61.8 ± 0.5
MCH (pg/cell)	28.2 ± 0.5	27.9 ± 0.7
MCHC (g/dl)	31.7 ± 0.4	32.5 ± 0.8
Platelet (10^3/μl)	91.2 ± 5.1	97.5 ± 3.5

Table 7
Organ functions and Serun Glucose, Serum Ca,NA,K, and Cl levels between the treated (50 μM/day) and control groups.

Parameter	Acute (50 μM/day)	Control (0)
AST (U/L)	102.3 ± 6.8	101.6 ± 8.5
ALT (U/L)	30.5 ± 6.5	31.6 ± 6.7
ALK PHOS (U/L)	80.4 ± 5.4	80.6 ± 4.4
BUN (mg/dl)	11.4 ± 1.6	10.5 ± 1.8
Creatinine (mg/dl)	0.62 ± 0.06	0.52 ± 0.03
Bilirubin Total (mg/dl)	0.62 ± 0.05	0.77 ± 0.02
Bilirubin Direct (mg/dl)	0.29 ± 0.03	0.25 ± 0.08
Bilirubin Indirect (mg/dl)	3.4 ± 0.24	3.1 ± 0.3
Albumin (g/dl)	4.25 ± 0.28	4.37 ± 0.45
Total protein (g/dl)	7.28 ± 0.15	7.36 ± 0.08
Glucose (mg/dl)	97.4 ± 6.5	97.8 ± 3.5
Ca (mg/dl)	10.2 ± 0.6	10.1 ± 0.6
Na (mEq/L)	142.6 ± 0.6	142.9 ± 0.7
K (mEq/L)	5.9 ± 0.9	5.9 ± 0.4
Cl (mEq/L)	102.5 ± 5.6	101.1 ± 5.9

Funding

The financial support was given by the ICMR (Grant No. 5/13/11/2020/NCD-III), Government of India.

Availability of data and materials

All data generated or analyzed during this study are included in this published article (and its supplementary information files)

Declaration of competing interest

The authors declare that they have no known competing financial interests or personal relationships that could have appeared to influence the work reported in this paper.

Data availability

All data generated or analysed during this study are included in this published article (and its supplementary information files)

Acknowledgement

The ICMR (Grant No. 5/13/11/2020/NCD-III) Govt. of India for providing the financial assistance.

Appendix A. Supplementary data

Supplementary data to this article can be found online at https://doi.org/10.1016/j.cbi.2023.110606.

References

[1] K. Ye, Y. Ke, N. Keshava, J. Shanks, J.A. Kapp, R.R. Tekmal, J. Petros, H.C. Joshi, Opium alkaloid noscapine is an antitumor agent that arrests metaphase and induces apoptosis in dividing cells, Proc. Natl. Acad. Sci. U. S. A. 95 (1998) 1601–1606.

[2] Y. Ke, K. Ye, H.E. Grossniklaus, D.R. Archer, H.C. Joshi, J.A. Kapp, Noscapine inhibits tumor growth with little toxicity to normal tissues or inhibition of immune responses, Cancer Immunol. Immunother. 49 (2000) 217–225.

[3] K. Ye, J. Zhou, J.W. Landen, E.M. Bradbury, H.C. Joshi, Sustained activation of p34 cdc2 is required for noscapine-induced apoptosis, J. Biol. Chem. 276 (2001) 46697–46700.
[4] E.K. Rowinsky, The development and clinical utility of the taxane class of antimicrotubule chemotherapy agents, Annu. Rev. Med. 48 (1997) 353–374.
[5] J. Zhou, P. Giannakakou, Targeting microtubules for cancer chemotherapy, Curr. Med. Chem. Anticancer Agents 5 (2005) 65–71.
[6] C. Theiss, K. Meller, Taxol impairs anterograde axonal transport of microinjected horseradish peroxidase in dorsal root ganglia neurons in vitro, Cell Tissue Res. 299 (2000) 213–224.
[7] K.S. Topp, K.D. Tanner, J.D. Levine, Damage to the cytoskeleton of large diameter sensory neurons and myelinated axons in vincristine-induced painful peripheral neuropathy in the rat, J. Comp. Neurol. 424 (2000) 563–576.
[8] J.W. Landen, R. Lang, S.J. McMahon, N.M. Rusan, A.M. Yvon, A.W. Adams, M. D. Sorcinelli, R. Campbell, P. Bonaccorsi, J.C. Ansel, D.R. Archer, P. Wadsworth, C. A. Armstrong, H.C. Joshi, Noscapine alters microtubule dynamics in living cells and inhibits the progression of melanoma, Cancer Res. 62 (2002) 4109–4114.
[9] J. Zhou, K. Gupta, S. Aggarwal, R. Aneja, R. Chandra, D. Panda, H.C. Joshi, Brominated derivatives of noscapine are potent microtubule-interfering agents that perturb mitosis and inhibit cell proliferation, Mol. Pharmacol. 63 (2003) 799–807.
[10] J. Zhou, K. Gupta, J. Yao, K. Ye, D. Panda, P. Giannakakou, H.C. Joshi, Paclitaxel-resistant human ovarian cancer cells undergo c-Jun NH2-terminal kinase-mediated apoptosis in response to noscapine, J. Biol. Chem. 277 (2002) 39777–39785.
[11] B. Dahlström, T. Mellstrand, C.-G. Löfdahl, M. Johansson, Pharmakokinetic properties of noscapine, Eur. J. Clin. Pharmacol. 22 (1982) 535–539.
[12] M.A. Oliva, A.E. Prota, J. Rodriguez-Salarichs, Y.L. Bennani, J. Jimenez-Barbero, K. Bargsten, A. Canales, M.O. Steinmetz, J.F. Diaz, Structural basis of noscapine activation for tubulin binding, J. Med. Chem. 63 (2020) 8495–8501.
[13] F. Couty, G. Evanoff, In Comprehensive heterocyclic chemistry III, in: A. R. Katritzky, C.A. Ramsden, E.F.V. Scriven (Eds.), RJK Taylor, vol. 11, Elsevier, Oxford, 2008.
[14] J. Liu, Q. Chen, Hua Xue Jin Zhan 22 (2010) 631;
(c) C. Enguehard-Gueiffier, A. Gueiffier, Mini-Rev. Med. Chem. 7 (2007) 888.
[15] J. Liu, Q. Chen, Hua Xue Jin Zhan 22 (2010) 631;
(c) J. Zhou, J. Liu, Q. Chen, Youji Huaxue 29 (2009) 1708.
[16] Y. Rival, G. Grassy, G. Michel, Synthesis and antibacterial activity of some Imidazo [1, 2-α] pyrimidine derivatives, Chem. Pharm. Bull. 40 (1992) 1170–1176.
[17] M.H. Fisher, A. Lusi, Imidazo [1, 2-a] pyridine anthelmintic and antifungal agents, J. Med. Chem. 15 (1972) 982–985.
[18] Y. Rival, G. Grassy, A. Taudou, R. Ecalle, Antifungal activity in vitro of some imidazo [1, 2-a] pyrimidine derivatives, Eur. J. Med. Chem. 26 (1991) 13–18.
[19] C. Hamdouchi, J. de Blas, M. del Prado, J. Gruber, B.A. Heinz, L. Vance, 2-Amino-3-substituted-6-[(E)-1-phenyl-2-(N-methylcarbamoyl) vinyl] imidazo [1, 2-a] pyridines as a novel class of inhibitors of human rhinovirus: stereospecific synthesis and antiviral activity, J. Med. Chem. 42 (1999) 50–59.
[20] J.J. Kaminski, A.M. Doweyko, Antiulcer agents. 6. Analysis of the in vitro biochemical and in vivo gastric antisecretory activity of substituted imidazo [1, 2-a] pyridines and related analogues using comparative molecular field analysis and hypothetical active site lattice methodologies, J. Med. Chem. 40 (1997) 427–436.
[21] S. Langer, S. Arbilla, J. Benavides, B. Scatton, Zolpidem and alpidem: two imidazopyridines with selectivity for omega 1-and omega 3-receptor subtypes, Adv. Biochem. Psychopharmacol. 46 (1990) 61–72.
[22] L. Almirante, L. Polo, A. Mugnaini, E. Provinciali, P. Rugarli, A. Biancotti, A. Gamba, W. Murmann, Derivatives of imidazole. I. Synthesis and reactions of imidazo [1, 2-α] pyridines with analgesic, antiinflammatory, antipyretic, and anticonvulsant activity, J. Med. Chem. 8 (1965) 305–312.
[23] R. Boerner, H. Moller, Saripidem-a new treatment for panic disorders, Psychopharmakotherapie 4 (1997) 145–148.
[24] R. Boerner, H. Moller, Psychopharmakotherapie 4 (1997) 145;
b) K. Gudmundsson, S.D. Boggs, PCT Int. Patent Appl. WO (2006), 2006026703.
[25] A.K. Patel, R.K. Meher, P.K. Reddy, R.K. Pedapati, P. Pragyandipta, S. Kantevari, M.R. Naik, P.K. Naik, Rational design, chemical synthesis and cellular evaluation of novel 1, 3-diynyl derivatives of noscapine as potent tubulin binding anticancer agents, J. Mol. Graph. Model. 106 (2021), 107933.
[26] P. Pragyandipta, M.R. Naik, B. Bastia, P.K. Naik, Development of 9-(N-arylmethylamino) congeners of noscapine: the microtubule targeting drugs for the management of breast cancer, 3 Biotech 13 (2023) 38.
[27] P.K. Naik, B.P. Chatterji, S.N. Vangapandu, R. Aneja, R. Chandra, S. Kanteveri, H. C. Joshi, Rational design, synthesis and biological evaluations of amino-noscapine: a high affinity tubulin-binding noscapinoid, J. Comput. Aided Mol. Des. 25 (2011) 443–454.
[28] R.A. Friesner, J.L. Banks, R.B. Murphy, T.A. Halgren, J.J. Klicic, D.T. Mainz, M. P. Repasky, E.H. Knoll, M. Shelley, J.K. Perry, D.E. Shaw, P. Francis, P.S. Shenkin, Glide: a new approach for rapid, accurate docking and scoring. 1. Method and assessment of docking accuracy, J. Med. Chem. 47 (2004) 1739–1749.
[29] T.A. Halgren, R.B. Murphy, R.A. Friesner, H.S. Beard, L.L. Frye, W.T. Pollard, J. L. Banks, Glide: a new approach for rapid, accurate docking and scoring. 2. Enrichment factors in database screening, J. Med. Chem. 47 (2004) 1750–1759.
[30] M.J. Abraham, T. Murtola, R. Schulz, S. Páll, J.C. Smith, B. Hess, E. Lindahl, GROMACS: high performance molecular simulations through multi-level parallelism from laptops to supercomputers, SoftwareX 1 (2015) 19–25.
[31] R. Kumar Pedapati, P. Pragyandipta, N. Pranathi Abburi, N. Chirra, S. Kantevari, P. K. Naik, Antiproliferative Noscapinoids Bearing an Amidothiadiazole Scaffold as Apoptosis Inducers: Design, Synthesis and Molecular Docking, Chem Biodivers, 2023, e202201089.
[32] V. Hornak, R. Abel, A. Okur, B. Strockbine, A. Roitberg, C. Simmerling, Comparison of multiple Amber force fields and development of improved protein backbone parameters, Proteins 65 (2006) 712–725.
[33] J. Wang, R.M. Wolf, J.W. Caldwell, P.A. Kollman, D.A. Case, Development and testing of a general amber force field, J. Comput. Chem. 25 (2004) 1157–1174.
[34] A. Jakalian, D.B. Jack, C.I. Bayly, Fast, efficient generation of high-quality atomic charges. AM1-BCC model: II. Parameterization and validation, J. Comput. Chem. 23 (2002) 1623–1641.
[35] A.W. Sousa da Silva, W.F. Vranken, Acpype - AnteChamber PYthon parser interfacE, BMC Res. Notes 5 (2012) 367.
[36] J.-P. Ryckaert, G. Ciccotti, H.J.C. Berendsen, Numerical integration of the cartesian equations of motion of a system with constraints: molecular dynamics of n-alkanes, J. Comput. Phys. 23 (1977) 327–341.
[37] P.A. Kollman, I. Massova, C. Reyes, B. Kuhn, S. Huo, L. Chong, M. Lee, T. Lee, Y. Duan, W. Wang, O. Donini, P. Cieplak, J. Srinivasan, D.A. Case, T. E. Cheatham 3rd, Calculating structures and free energies of complex molecules: combining molecular mechanics and continuum models, Acc. Chem. Res. 33 (2000) 889–897.
[38] R. Kumari, R. Kumar, C. Open, Source Drug Discovery, A. Lynn, g_mmpbsa–a GROMACS tool for high-throughput MM-PBSA calculations, J. Chem. Inf. Model. 54 (2014) 1951–1962.
[39] M.M. Tomayko, C.P. Reynolds, Determination of subcutaneous tumor size in athymic (nude) mice, Cancer Chemother. Pharmacol. 24 (1989) 148–154.
[40] R. Aneja, S.N. Vangapandu, M. Lopus, V.G. Viswesarappa, N. Dhiman, A. Verma, R. Chandra, D. Panda, H.C. Joshi, Synthesis of microtubule-interfering halogenated noscapine analogs that perturb mitosis in cancer cells followed by cell death, Biochem. Pharmacol. 72 (2006) 415–426.
[41] R. Aneja, S.N. Vangapandu, M. Lopus, R. Chandra, D. Panda, H.C. Joshi, Development of a novel nitro-derivative of noscapine for the potential treatment of drug-resistant ovarian cancer and T-cell lymphoma, Mol. Pharmacol. 69 (2006) 1801–1809.
[42] N. Jain, D. Yada, T.B. Shaik, G. Vasantha, P.S. Reddy, S.V. Kalivendi, B. Sreedhar, Synthesis and antitumor evaluation of nitrovinyl biphenyls: anticancer agents based on allocolchicines, ChemMedChem 6 (2011) 859–868.
[43] S. Santoshi, N.K. Manchukonda, C. Suri, M. Sharma, B. Sridhar, S. Joseph, M. Lopus, S. Kantevari, I. Baitharu, P.K. Naik, Rational design of biaryl pharmacophore inserted noscapine derivatives as potent tubulin binding anticancer agents, J. Comput. Aided Mol. Des. 29 (2015) 249–270.